AMERICAN SOCIETY FOR MICROBIOLOGY | mBio®

RESEARCH ARTICLE

ATP Drives Efficient Terpene Biosynthesis in Marine Thraustochytrids

Aiqing Zhang,[a,b] Kaya Mernitz,[b] Chao Wu,[c] Wei Xiong,[c] Yaodong He,[a,b] Guangyi Wang,[a,d] Xin Wang[b]

[a]School of Environmental Science and Engineering, Tianjin University, Tianjin, China
[b]Department of Microbiology, Miami University, Oxford, Ohio, USA
[c]Biosciences Center, National Renewable Energy Laboratory, Golden, Colorado, USA
[d]Key Laboratory of Systems Bioengineering (Ministry of Education), Tianjin University, Tianjin, China

ABSTRACT Understanding carbon flux controlling mechanisms in a tangled metabolic network is an essential question of cell metabolism. Secondary metabolism, such as terpene biosynthesis, has evolved with low carbon flux due to inherent pathway constraints. Thraustochytrids are a group of heterotrophic marine unicellular protists and can accumulate terpenoids under the high-salt conditions in their natural environment. However, the mechanism behind terpene accumulation is not well understood. Here, we show that terpene biosynthesis in *Thraustochytrium* sp. ATCC 26185 is constrained by local thermodynamics in the mevalonate pathway. Thermodynamic analysis reveals metabolite limitation in the nondecarboxylative Claisen condensation of acetyl-coenzyme A (CoA) to the acetoacetyl-CoA step, catalyzed by the acetyl-CoA acetyltransferase (ACAT). Through a sodium-elicited mechanism, higher respiration leads to increased ATP investment into the mevalonate pathway, providing a strong thermodynamic driving force for enhanced terpene biosynthesis. Proteomic and metabolomic analyses further show that the increased ATP demands are fulfilled by shifting energy generation from carbohydrate to lipid oxidation. This study demonstrates a unique strategy in nature that uses ATP to drive a low-flux metabolic pathway, providing an alternative solution for efficient terpene metabolic engineering.

IMPORTANCE Terpenoids are a large class of lipid molecules with important biological functions and diverse industrial and medicinal applications. Metabolic engineering for terpene production has been hindered by the low-flux distribution to its biosynthesis pathway. In practice, a high substrate load is generally required to reach high product titers. Here, we show that mevalonate-derived terpene biosynthesis is constrained by local pathway thermodynamics, which can only be partially relieved by increasing substrate levels. Through comparative omics and biochemical analyses, we discovered a unique mechanism for high terpene accumulation in marine protist thraustochytrids. Through a sodium-induced mechanism, thraustochytrids shift their energy metabolism from carbohydrate to lipid oxidation for enhanced ATP production, providing a strong thermodynamic driving force for efficient terpene biosynthesis. This study reveals an important mechanism in eukaryotes to overcome the thermodynamic constraint in low-flux pathways by increased ATP consumption. Engineering energy metabolism thus provides an important alternative to relieve flux constraints in low-flux and energy-consuming pathways.

KEYWORDS thermodynamics, terpene metabolism, β-oxidation, squalene, thraustochytrids, mevalonate pathway

Terpenoids are a large class of secondary metabolites produced by plants and microbes (1). Two C_5 terpene precursors, isopentenyl diphosphate (IPP) and dimethylallyl diphosphate (DMAPP), can be condensed into diverse classes of terpene

Citation Zhang A, Mernitz K, Wu C, Xiong W, He Y, Wang G, Wang X. 2021. ATP drives efficient terpene biosynthesis in marine thraustochytrids. mBio 12:e00881-21. https://doi.org/10.1128/mBio.00881-21.

Invited Editor Yinjie J. Tang, Washington University in St. Louis

Editor Edward G. Ruby, University of Hawaii at Manoa

Address correspondence to Guangyi Wang, gywang@tju.edu.cn, or Xin Wang, xwang@miamioh.edu.

Received 24 March 2021
Accepted 19 May 2021
Published 29 June 2021

molecules, which include monoterpenes (C_{10}), diterpenes (C_{20}), triterpenes (C_{30}), and so forth (2). Many terpenoids participate in a variety of biological processes, including cell wall biosynthesis, membrane function, electron transport, and conversion of light energy into chemical energy (3). The triterpene squalene ($C_{30}H_{50}$) is an important intermediate during cholesterol biosynthesis in eukaryotic cells (4). Squalene has shown great potential for medical applications, including suppressing colon carcinogenesis (5), improving immune system health (6), and enhancing drug and vaccine delivery as parenteral emulsions (7).

The livers of deep-sea sharks are among the main commercial squalene sources, containing 15 to 69% by weight of squalene (8). However, harvesting sharks is not a sustainable solution for squalene supply. Metabolic engineering of microbes and plants thus serves as a valuable alternative to supply sustainable squalene to the market. However, engineering high terpene yields is challenging due to inherent flux constraints within the terpene biosynthesis pathway. In eukaryotes, the mevalonate pathway is mainly responsible for generating the terpene precursors IPP and DMAPP (9, 10). Three acetyl-coenzyme A (CoA) molecules are sequentially condensed into one IPP in six steps, consuming three ATP and two NADPH in total. IPP can then be converted to DMAPP by IPP isomerase (11). To generate squalene, IPP and DMAPP are fused to form farnesyl diphosphate (FPP) by FPP synthase, followed by a head-to-head FPP addition into presqualene diphosphate (PSPP), and a reductive rearrangement to convert PSPP to squalene catalyzed by squalene synthase (12).

Two key factors govern the flux distribution into metabolic pathways, i.e., thermodynamics and enzyme kinetics. Due to the low carbon flux distribution into terpene biosynthesis, a high substrate load is generally necessary to provide a favorable thermodynamic driving force for high terpene titers. Pathway yield can be further enhanced through kinetic improvement where rate-limiting enzymes are targeted for optimization of their expression levels. The 3-hydroxy-3-methylglutaryl CoA reductase (HMGR) is widely recognized as the key enzyme in the mevalonate pathway to improve terpene flux through gene overexpression (13). Diverting carbon flux from competing metabolic processes into terpene biosynthesis can also effectively increase terpene flux (14). For intermediary terpene metabolites such as squalene, the loss of the product yield can be attributed to squalene consumption by downstream metabolism (15). Strategies such as product sequestering thus are often implemented to improve terpene yield. In plants, sequestering squalene into a lipid droplet has shown improved squalene yield (16).

Understanding the carbon flux controlling mechanism in an organism with native high terpene flux could provide valuable insight for terpene engineering. The marine protist thraustochytrids can accumulate high levels of terpenes such as squalene and carotenoids (17–19). The strain *Aurantiochytrium* sp. 18W-13a accumulated squalene up to 17% of cell dry weight under optimized fermentation conditions (20). Several other thraustochytrid strains, including *Aurantiochytrium* sp. TWZ-97 (21), *Schizochytrium mangrovei* PQ6 (22), and *S. limacinum* SR21 (23), also showed great potential for squalene production. In thraustochytrids, sodium was proposed to contribute largely to the osmotic adjustment but not to cell physiology (24). In this study, we found that sodium elicits increased respiration rates in *Thraustochytrium* sp. ATCC 26185 (hereafter *Thraustochytrium* sp.), leading to increased ATP investment in the mevalonate pathway and high squalene yield. The discovery of ATP directly driving terpene biosynthesis provides important insight for future terpene-engineering efforts.

RESULTS

NaCl stimulates squalene accumulation during cell growth. Thraustochytrids require sodium for cell growth in the marine environment. To show how sodium affects cell growth and lipid metabolism in *Thraustochytrium* sp., we grew cells with 5 g/liter NaCl or without supplementing medium with NaCl. Compared to cells grown in the sodium-supplemented medium (NaCl-5), cells without sodium (NaCl-0) showed a small lag phase during growth (Fig. 1A and B). However, the final biomass accumulation was similar under both conditions,

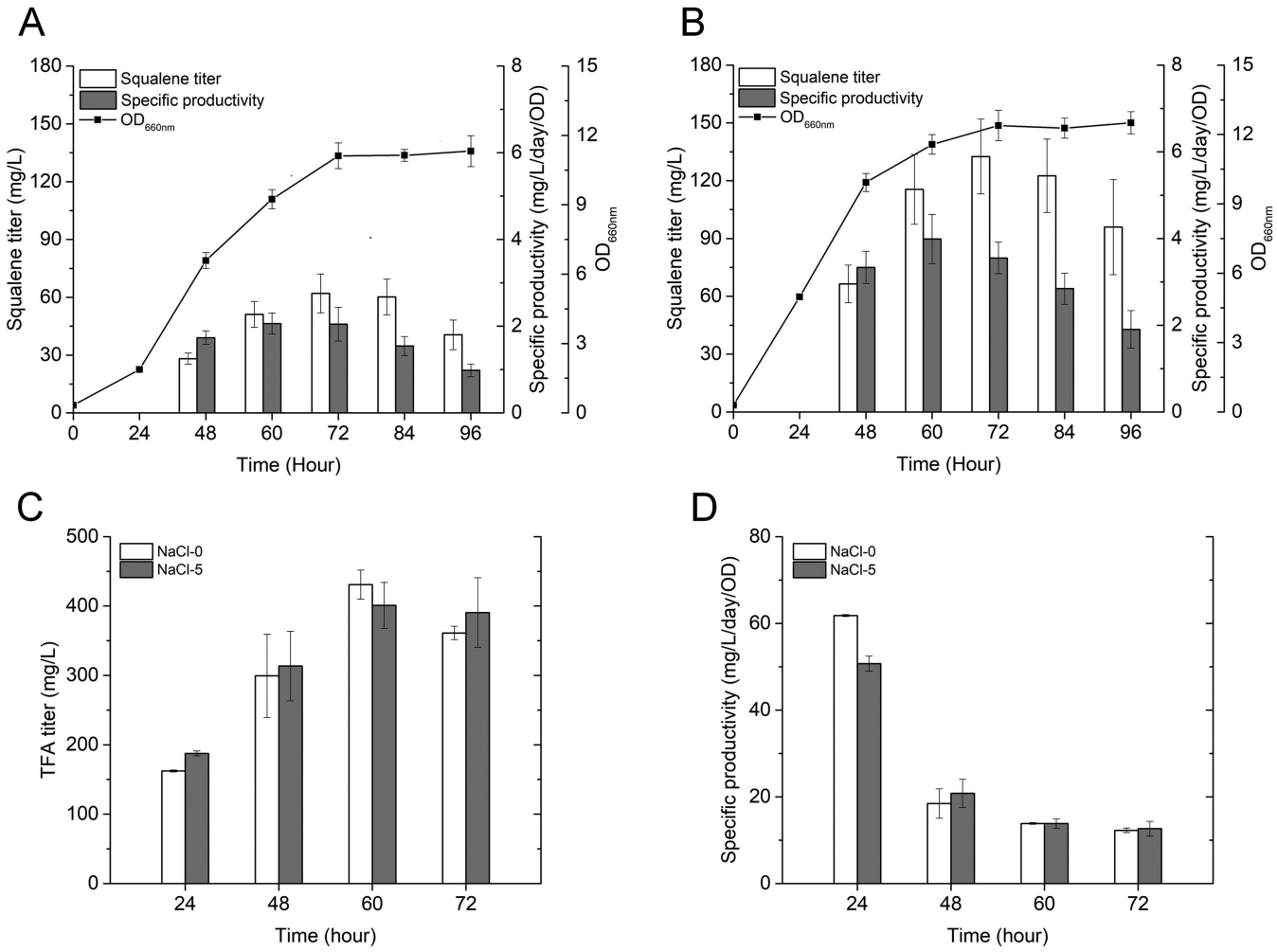

FIG 1 Growth and lipid production of *Thraustochytrium* sp. ATCC 26185 under different NaCl conditions. Squalene production and cell growth of cells cultivated (A) without NaCl (NaCl-0) and (B) with 5 g/liter NaCl (NaCl-5). Total fatty acids (TFA) titer (C) and specific productivity (D) of cells grown with or without NaCl.

reaching the maximum optical density (OD) of ~12 after 72 h of growth. On the other hand, squalene accumulation was significantly higher under the sodium supplementation condition. Under both conditions, the squalene titer in *Thraustochytrium* sp. reached the highest level in the beginning of the stationary phase. The highest squalene titer was 123.6 mg/liter in the NaCl-5 group (Fig. 1B), a 2-fold increase ($P < 0.01$) compared to the titer in the NaCl-0 group (Fig. 1A and B). The specific squalene productivity was highest ($P < 0.01$) after 60 h of growth, reaching 4 and 2.1 mg/liter/day/OD in the NaCl-5 and NaCl-0 groups, respectively (Fig. 1A and B). To understand whether increased squalene production results from sodium specifically or from osmotic regulation in general, we substituted NaCl with the same molar concentration of KCl in the growth medium to reach the same osmotic level. Interestingly, cells grown with or without KCl supplementation had similar squalene titers and productivity levels, which were significantly lower than those of cells grown with NaCl supplementation (see Fig. S1 in the supplemental material), indicating a sodium-specific induction mechanism for squalene accumulation in *Thraustochytrium* sp.

Fatty acid biosynthesis consumes the same precursor acetyl-CoA as mevalonate-derived squalene biosynthesis. If the increased squalene biosynthesis is due to higher acetyl-CoA levels under the salt supplementation condition, we could expect to see an increase in the total fatty acids (TFA). To understand how sodium affects fatty acid production, we measured the TFA contents in the NaCl-0 and NaCl-5 cells. The TFA analysis revealed the accumulation of a variety of fatty acids with different carbon lengths,

including myristic acid ($C_{14:0}$), pentadecylic acid ($C_{15:0}$), palmitic acid ($C_{16:0}$), margaric acid ($C_{17:0}$), stearic acid ($C_{18:0}$), and docosahexaenoic acid ($C_{22:6}$) (see Table S1 in the supplemental material). Although *Thraustochytrium* sp. cells showed a slight variation in their composition of C_{14}, C_{15}, and C_{16} fatty acids, both TFA titer and specific productivity were similar under two growth conditions, with and without sodium supplementation (Fig. 1C and D and Table S1). The TFA titer had the highest level after 60 h of cell growth, reaching 430.9 mg/liter without NaCl and 401 mg/liter with NaCl (Fig. 1C). TFA specific productivity was highest at the 24-h time point for both conditions, and it decreased significantly when cells reached higher densities.

NaCl induces a shift in energy metabolism that benefits ATP-consuming pathways. To understand how sodium affects cell metabolism in *Thraustochytrium* sp., we conducted comparative proteomics on cells grown under two growth conditions (with and without sodium supplementation). The cells with the highest specific squalene productivity (at 60 h) were used for the proteomic analysis. For each growth condition, an average of about 1,000 proteins were identified from the proteomics. Proline and glutamate are two commonly known compatible solutes for osmotic adjustment. In our proteomic analysis, ornithine aminotransferase (OAT) and delta-1-pyrroline-5-carboxylate dehydrogenase (P5CDH), two key enzymes catalyzing the generation of proline and glutamate, showed significantly higher levels in cells grown with sodium (Fig. 2), indicating their potential involvement in the osmotic adjustment in *Thraustochytrium* sp.

Under the salt supplementation condition, key enzymes in the Embden-Meyerhof-Parnas (EMP) pathway and the fatty acid synthesis pathway showed significantly lower abundances compared to those in cells grown without sodium (Fig. 2A and B). Hexokinase (HK) and fructose-bisphosphate aldolase (ALDO) showed 2.1- and 1.7-fold decreases in enzyme levels when cells grew under the salt supplementation condition. The protein abundance of phosphoglycerate kinase (PGK), the enzyme catalyzing one of the substrate-level phosphorylation steps in the EMP pathway, decreased 2-fold when cells were grown under the salt supplementation condition. In addition, two subunits of the pyruvate dehydrogenase complex, the enzyme responsible for the conversion of pyruvate to acetyl-CoA, had significantly lower abundances in cells grown under the salt supplementation condition, suggesting a lower flux toward acetyl-CoA generation through glucose catabolism. Interestingly, key enzymes for fatty acid biosynthesis also showed decreased levels in cells grown under the salt supplementation condition. Two pathways are responsible for fatty acid synthesis in thraustochytrids, i.e., the fatty acid synthase I (FAS I) system and the polyketide synthase-like (PKS-like) pathway (25). In cells grown under the salt supplementation condition, acetyl-CoA carboxylase (ACC), FAS I subunit alpha, and FAS I subunit beta showed 1.6-, 2.3-, and 2.5-fold decreases in their protein abundances, respectively. The components of the PKS-like pathway did not show differences in their protein levels. The above-described observations suggest a decreased carbon flux from glucose catabolism and a lower fatty acid synthesis activity in *Thraustochytrium* sp. under the salt supplementation condition.

On the other hand, the acyl-CoA dehydrogenase (ACAD), a key enzyme in the β-oxidation pathway (26), showed a 2.2-fold enzyme increase in cells grown under the salt supplementation condition (Fig. 2A and B). The higher ACAD level suggests an enhanced ATP generation through the more efficient lipid oxidation when sodium is supplemented into the growth medium. A lipid transfer protein also showed 1.8-fold protein increase under the sodium supplementation condition, suggesting its possible involvement in transferring fatty acids from the cytosol to the mitochondria for lipid degradation. These drastic changes in the enzymes associated with energy generation showed a clear shift from carbohydrate to lipid oxidation when the cells were grown under the salt supplementation condition.

The lipid degradation through β-oxidation could also lead to higher acetyl-CoA levels, benefiting acetyl-CoA consuming processes such as mevalonate-derived terpene biosynthesis (27). Interestingly, the proteomic analysis showed significantly increased

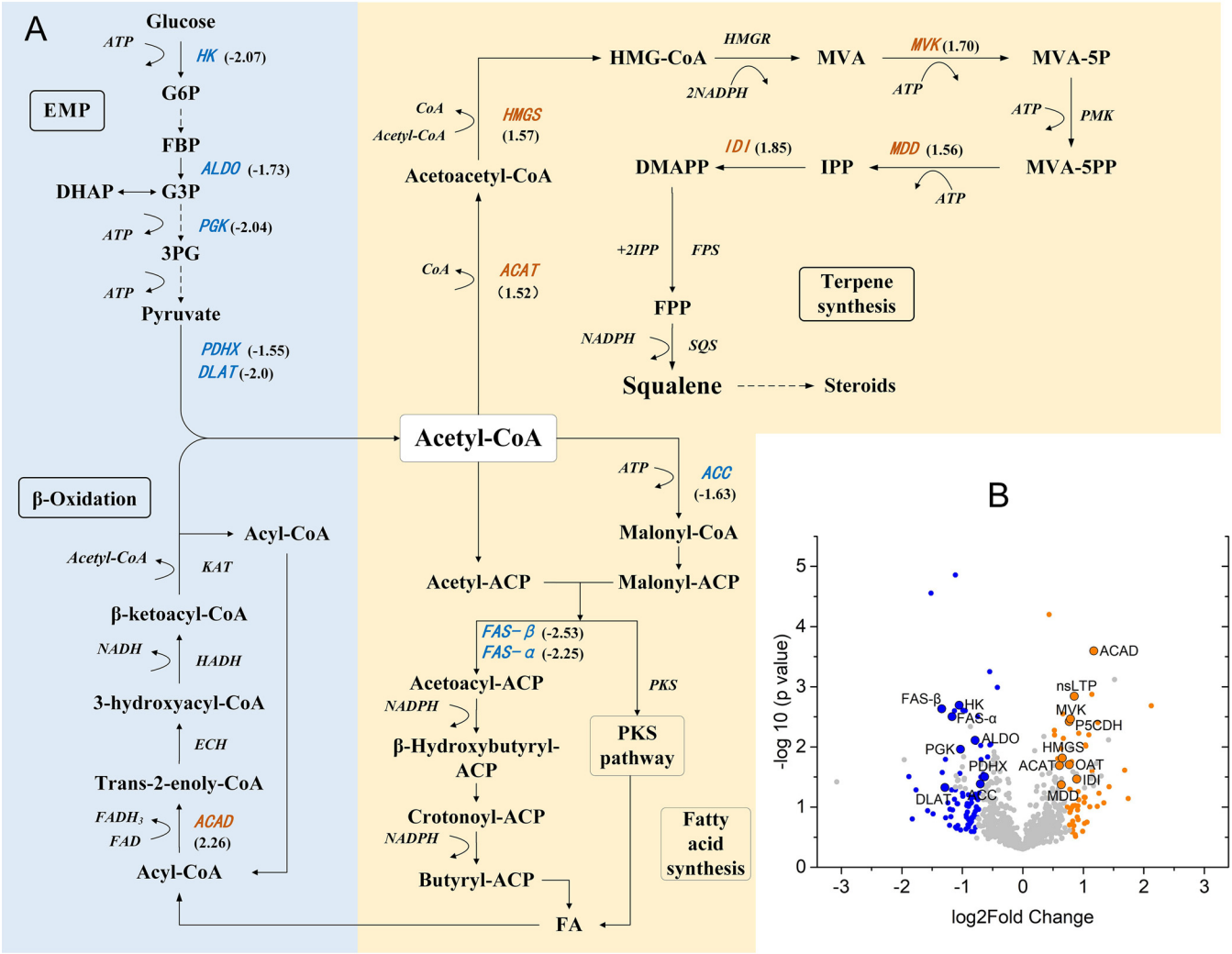

FIG 2 Sodium elicits an energy metabolism shift in *Thraustochytrium* sp. (A) Pathway diagram showing squalene synthesis from either glucose or lipid oxidation. Enzymes with statistically different levels in the comparative proteomic analysis are shown in blue (decreased) and orange (increased), with the relative fold change in brackets. Enzymes: HK, hexokinase; ALDO, fructose-bisphosphate aldolase; PGK, phosphoglycerate kinase; PK, pyruvate kinase; PDHX, pyruvate dehydrogenase protein X component; DLAT, dihydrolipoyllysine-residue acetyltransferase component of pyruvate dehydrogenase complex; ACAT, acetyl-coenzyme A (CoA) acetyltransferase; HMGS, 3-hydroxy-3-methylglutaryl-CoA synthase; HMGR, 3-hydroxy-3-methylglutaryl-CoA reductase; MVK, mevalonate kinase; PMK, phosphomevalonate kinase; MDD, diphosphomevalonate decarboxylase; ACAD, acyl-CoA dehydrogenase; ECH, enoyl-CoA hydratase; HADH, 3-hydroxyacyl-CoA dehydrogenase; KAT, 3-ketoacyl-CoA thiolase; IDI, isopentenyl-diphosphate isomerase; FPS, farnesyl diphosphate synthase; SQS, squalene synthase; FAS-α, fatty acid synthase subunit alpha; FAS-β, fatty acid synthase subunit beta. Metabolites: G6P, D-glucose 6-phosphate; FBP, D-fructose 1,6-bisphosphate; G3P, D-glyceraldehyde 3-phosphate; 3PG, 3-phospho-D-glyceroyl phosphate; HMG-CoA, (*S*)-3-hydroxy-3-methylglutaryl-CoA; MVA, mevalonate; MVA-5P, mevalonate-5-phosphate; MVA-5PP, mevalonate-5-pyrophosphate; IPP, isopentenyl diphosphate; DMAPP, dimethylallyl diphosphate; FPP, farnesyl diphosphate; FA, fatty acid. (B) Volcano plot of the whole proteome. Orange and blue dots represent proteins with significantly increased and decreased levels, respectively, when sodium is supplemented in the growth medium. Gray dots represent proteins with similar protein levels under two growth conditions. Enzymes and proteins: OAT, ornithine aminotransferase; P5CDH, delta-1-pyrroline-5-carboxylate dehydrogenase; nsLTP, nonspecific lipid transfer protein.

levels of mevalonate pathway enzymes in cells grown with sodium. Specifically, the enzyme abundances of acetyl-CoA acetyltransferase (ACAT), 3-hydroxy-3-methylglutaryl-CoA synthase (HMGS), mevalonate kinase (MVK), and mevalonate diphosphate decarboxylase (MDD), increased by 1.5-, 1.6-, 1.7-, and 1.6-fold, respectively, when cells were grown with sodium. The above-described results indicate a higher flux toward terpene biosynthesis under the salt supplementation condition. The energy metabolism shift from carbohydrate to lipid oxidation thus could potentially benefit terpene biosynthesis, either through the increased acetyl-CoA input or ATP generation.

Carbon metabolism shift from carbohydrate to lipid oxidation is beneficial for osmotic adjustment. To better understand the proteomic results, we conducted a comparative metabolomic study on thraustochytrid cells with the highest specific

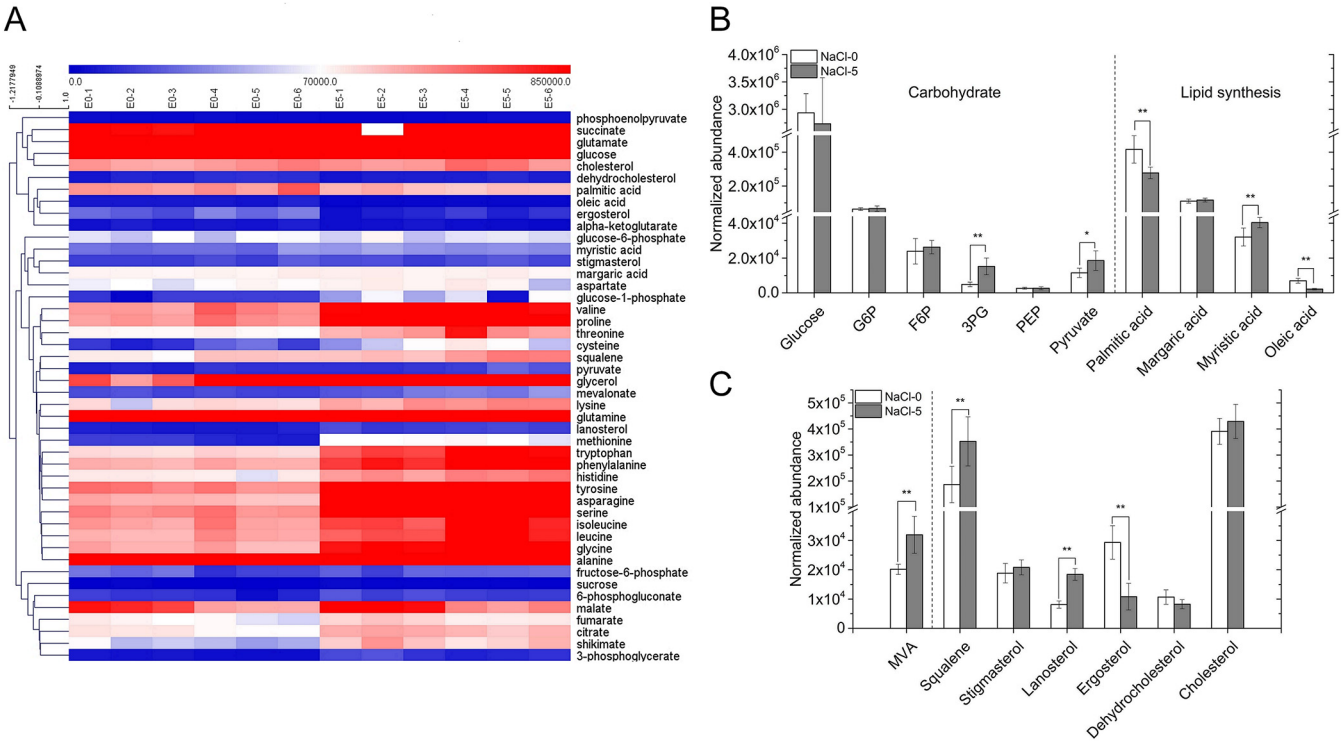

FIG 3 Comparative metabolomics supports energy metabolism shift from carbohydrate to lipid oxidation. (A) Heatmap shows changes of essential metabolites from the central metabolism under two growth conditions (with and without sodium supplementation). (B) Embden-Meyerhof-Parnas (EMP) pathway intermediates and fatty acid levels indicate degradation of lipids and sustained 3PG and pyruvate levels for amino acid synthesis. (C) Metabolite levels from the mevalonate pathway and downstream terpenoid biosynthesis pathways. *, $P < 0.05$; **, $P < 0.01$.

squalene productivity (at 60 h). Among the identified metabolites, about 50 are those from the EMP, citric acid cycle, amino acid synthesis, fatty acid synthesis, and terpene synthesis pathways (Fig. 3A). Six intermediates from the EMP pathway, i.e., glucose, D-glucose 6-phosphate (G6P), fructose 6-phosphate (F6P), 3-phosphoglycerate (3PG), phosphoenolpyruvate (PEP), and pyruvate, were detected and showed differing abundances between cells grown with or without sodium. More specifically, four intermediates (glucose, G6P, F6P, and PEP) were found in similar abundances under these two growth conditions; however, 3PG and pyruvate were found to be 3.1- and 1.6-fold more abundant in cells grown with sodium (Fig. 3A and B). Interestingly, 3PG and pyruvate are two of the EMP pathway intermediates that serve as outlets for the synthesis of several amino acids, including serine, glycine, cysteine, alanine, valine, leucine, and isoleucine (28). The metabolomic results further show that all of these amino acids had significantly higher abundances in cells grown with sodium (Fig. 3A; see also Fig. S2 in the supplemental material. Together with the proteomic results showing that lower abundances of HK, ALDO, and PGK were found in cells grown with sodium (Fig. 2), these data support the conclusion of a lower catabolic flux from glucose to 3PG. It would appear that increased 3PG and pyruvate arose from the gluconeogenesis process for amino acid synthesis. On the other hand, a few fatty acids, including palmitic acid ($C_{16:0}$), margaric acid ($C_{17:0}$), myristic acid ($C_{14:0}$), and oleic acid ($C_{18:1}$), were found to have similar or lower abundances in cells grown with sodium (Fig. 3A and B). Consistent with the TFA analysis (Fig. 1C and D), palmitic acid was found to be the most abundant fatty acid component in the metabolome, and it was 1.5-fold lower in cells grown with sodium (Fig. 3B). A similar result was observed for the unsaturated oleic acid, whose abundance only accounts for a small portion of the TFA but decreased 3.2-fold in cells grown with sodium (Fig. 3B). These results support the conclusion of energy generation from lipid degradation rather than glycolysis by the EMP pathway, benefiting ATP-consuming metabolic processes.

The metabolomic analysis further showed increased flux in the mevalonate pathway and increased accumulation of squalene and downstream steroids in cells grown with sodium (Fig. 3A and C). The amount of mevalonate and squalene were found to be 1.6- and 1.9-fold higher in cells grown with sodium, consistent with the quantitative squalene determination result (Fig. 1A and B). In addition, we also observed several downstream steroids in the metabolomic analysis, including lanosterol, dehydrocholesterol, cholesterol, ergosterol, and stigmasterol (Fig. 3A and C). All of these downstream steroids, except for ergosterol, showed either similar or higher abundances in cells grown with sodium. Cholesterol was the most abundant downstream steroid detected and had slightly higher abundance in cells grown with sodium. Ergosterol accounts for a relatively small portion of the detected steroids and had lower abundance in cells grown with sodium, likely caused by further conversion to downstream metabolites such as vitamin D_2 (29). The metabolomic results further support the hypothesis that carbon metabolism shift from carbohydrate to lipid degradation benefits the mevalonate-derived terpene biosynthesis. It is worth mentioning that terpene synthesis is a low-flux pathway. Although the metabolite increase is significant for terpenes *per se*, it might only account for a relatively small decrease in fatty acids, which explains the similar TFA abundances between cells grown with or without sodium (Fig. 1C and D). In addition, metabolomic analysis reflects a snapshot of cellular activities and might not accurately predict the flux change in certain metabolic pathways. Combined with measurements of product titers and enzyme abundances through techniques such as proteomics, these combinatorial analyses could thus provide more accurate predictions of carbon flux changes.

The comparative metabolomic analysis further provides insight about potential association between osmotic adjustment and the shift of carbon metabolism. In the metabolomics results, glutamate and proline, two of the common compatible solutes, were 1.4- and 6.1-fold more abundant, respectively, in cells grown with sodium (Fig. S2). Biosynthesis of amino acids is generally coordinated to ensure balance for protein synthesis (30). The increase in glutamate and proline seems to have led to the increase of all other amino acids and their precursors (Fig. 3A and Fig. S2). Collectively, these results suggest that *Thraustochytrium* sp. depends on compatible amino acids for osmotic adjustment, which benefits from the carbon metabolism shift from carbohydrate to lipid degradation. Shifting from glycolysis to the more efficient lipid β-oxidation for reducing equivalent generation used in cellular respiration will fulfill both the energy requirement by cellular activities and maintain central metabolism intermediates for amino acid biosynthesis.

***In silico* analysis reveals local thermodynamic constraint in squalene biosynthesis.** The proteomic and metabolomic analyses suggest an energy metabolism shift from carbohydrate to lipid degradation in *Thraustochytrium* sp., which could lead to increased acetyl-CoA and ATP generation. To understand how the generation of acetyl-CoA and ATP could benefit terpene biosynthesis, we investigated the thermodynamic landscape of squalene biosynthesis using the pathway analysis tool PathParser (31). PathParser is able to identify the step of a metabolic pathway whose flux is constrained by thermodynamics under physiological conditions. By optimizing metabolite concentrations for all reactions within the defined concentration range (1 μM to 10 mM), PathParser seeks to obtain a set of metabolite concentrations that can maximize the driving force of the whole pathway. Under optimized conditions, the metabolic step whose substrates/products concentrations most closely approaches the defined concentration boundaries is thus identified as the thermodynamic bottleneck step.

In the thermodynamic modeling, either glycolysis or β-oxidation of a short-chain fatty acid hexanoyl-CoA was used as the upstream pathway for squalene synthesis. Interestingly, the optimized squalene synthesis pathway is constrained by the ACAT-catalyzed reaction, regardless of the upstream catabolic processes (Fig. 4). ACAT catalyzes the nondecarboxylative Claisen condensation of two molecules of acetyl-CoA into acetoacetyl-CoA in the mevalonate pathway. The optimized ACAT reaction has a Gibbs free energy change ($\Delta G'$) of -1.69 kJ/mol with glucose as the starting substrate and a $\Delta G'$ of near 0 kJ/mol when hexanoyl-CoA serves as the starting substrate (see Tables S2 and S3 in the supplemental material). In particular, the reaction is constrained by both the upper bound (10 mM) of acetyl-

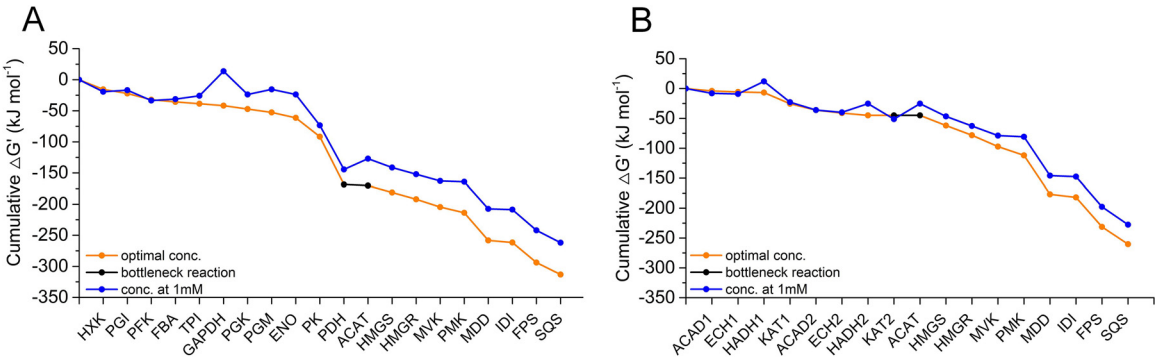

FIG 4 Thermodynamic landscape of squalene synthesis from either carbohydrate or short-chain fatty acid. *In silico* analysis of squalene synthesis from glucose (A) and a short-chain fatty acid, hexanoyl-CoA (B). The blue line denotes standard Gibbs free energy at physiological 1 mM concentrations of metabolites. The orange line denotes reactions with optimized metabolite concentrations to provide maximal driving force for the whole pathway. The black line indicates the thermodynamic-constrained bottleneck reaction in the pathway, in which both the substrate acetyl-CoA and the product acetoacetyl-CoA are approaching their concentration boundaries (1 μM to 10 mM) under the optimized conditions.

CoA concentration and the lower bound (1 μM) of acetoacetyl-CoA concentration, as both metabolites are approaching their concentration limits under the optimized conditions (see Table S4 in the supplemental material). Under physiological conditions, the metabolite concentration is seldom higher than 10 mM or lower than 1 μM, which indicates a thermodynamic limitation in the mevalonate-derived terpene biosynthesis pathway. In fact, if the concentration of coenzyme A increases to 5 mM instead of the defined 1 mM, the ACAT-catalyzed reaction becomes infeasible, with positive $\Delta G'$ values for both glucose- and hexanoyl-CoA-derived squalene synthesis (see Tables S5, S6, and S7 in the supplemental material). These analyses show that the ACAT-catalyzed reaction operates near equilibrium under optimized physiological conditions and would require high enzyme kinetics (k_{cat}/K_m) in order to sustain a forward net flux (32).

Both glycolysis and β-oxidation can lead to the production of acetyl-CoA, which can be transported out of the mitochondria for terpene synthesis in the cytosol. The thermodynamic analysis also indicates inefficiency in driving the mevalonate pathway by increasing the acetyl-CoA concentration. In reality, the measured acetyl-CoA concentration in eukaryotic cells is in the micromolar range (33), several hundredfold lower than the concentration used in the modeling. Increasing carbon flux of the mevalonate pathway would require significantly high steady-state acetyl-CoA pools or extremely low acetoacetyl-CoA pools to provide a strong thermodynamic driving force. We further measured acetyl-CoA levels of *Thraustochytrium* sp. cells grown under both growth conditions. At all measured time points, acetyl-CoA levels were similar in cells grown with or without sodium supplementation (Fig. 5A), showing that it is not an

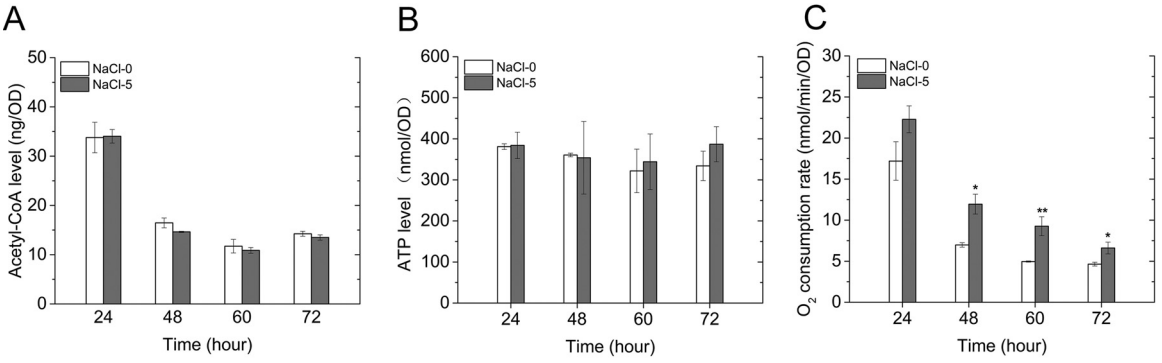

FIG 5 Acetyl-CoA pools and energy status of *Thraustochytrium* sp. under different growth conditions (with and without sodium supplementation). Acetyl-CoA pools (A), ATP levels (B), and respiration rates (C) were measured along with cell growth with or without NaCl supplemented in the medium. *, $P < 0.05$; **, $P < 0.01$.

increase of acetyl-CoA pools providing the driving force. How can cells then benefit from switching to lipid oxidation to synthesize terpenoids? Besides acetyl-CoA, lipid β-oxidation also generates the reducing equivalents $FADH_2$ and NADH, which can directly participate in the electron transport chain for ATP production. On the other hand, the mevalonate pathway has three ATP-dependent steps that are catalyzed by MVK, phosphomevalonate kinase (PMK), and MDD. It is tempting to assume that efficient ATP production could provide a strong thermodynamic driving force for the mevalonate pathway, which can help alleviate the upstream thermodynamic constraint in the ACAT-catalyzed step.

NaCl stimulates increased ATP production and drives efficient squalene synthesis. To verify whether ATP production can provide a strong thermodynamic driving force for squalene biosynthesis, we first measured the ATP levels in cells grown with or without 5 g/liter of NaCl. Surprisingly, the ATP concentration remained at similar levels throughout cell growth (Fig. 5B), indicating a tight cellular regulation to achieve energy homeostasis. The measured ATP level represents only the steady-state metabolite profile and does not reflect its dynamic changes. We thus measured cellular respiration by looking at oxygen consumption rates. Under both growth conditions, the oxygen consumption rates decreased along with cell growth. In addition, the oxygen consumption rates showed similar levels at the 24-h time point between cells grown with and without sodium. However, the oxygen consumption rates were significantly higher in cells grown with sodium than in those without sodium after 24 h of cultivation. At all three time points (48 h, 60 h, and 72 h), the respiration rates of NaCl-5 cells were 1.7-, 1.8-, and 1.5-fold higher, respectively, in comparison with those of the NaCl-0 cells (Fig. 5C). This observation strongly supports our hypothesis that increased ATP generation leads to enhanced terpene production in *Thraustochytrium* sp. Collectively, the computational modeling and metabolite analyses indicate that coupling the lower part of the mevalonate pathway reactions with ACAT-catalyzed acetyl-CoA condensation is critical to reduce the acetoacetyl-CoA level enough to enable an overall thermodynamically favorable mevalonate pathway reaction.

DISCUSSION

The yield of a target compound is determined by the carbon flux distributed to its biosynthesis pathway. Both enzyme kinetics and thermodynamics determine carbon flux distribution in metabolic pathways. The flux control coefficient (C) shows the relative contribution of a specific enzyme to the overall pathway flux. Kinetic bottlenecks can be alleviated through enzyme overexpression or by substitution with enzyme homologs of higher activities (34). The contribution of thermodynamics to pathway flux is not widely appreciated. Not only does thermodynamics determine the feasibility of a reaction, but it also constrains the pathway kinetics according to the flux-force relationship (32, 35). When a reaction approaches equilibrium, i.e., the Gibbs free energy change ($\Delta G'$) approaches 0, a large portion of the enzymes is used to catalyze the reverse reaction. A substantial increase in enzyme numbers is thus required to sustain the net flux. We show in this study that terpene synthesis is constrained by local pathway thermodynamics in the mevalonate pathway, which can be relieved by elevated expression of pathway enzymes (Fig. 2) and by increased ATP production through a sodium-elicited mechanism in *Thraustochytrium* sp. The concomitant shift of acetyl-CoA and ATP generation pathways provides a strong thermodynamic driving force for the mevalonate pathway, leading to enhanced squalene biosynthesis in *Thraustochytrium* sp. (Fig. 1).

Pathway constraints by local thermodynamics are not uncommon in nature. For instance, many of the carbon fixation pathways in nature consume more ATP than what is necessary to make the overall reaction thermodynamically favorable. It has been found that two types of reactions, i.e., carboxylation and carboxyl reduction, are energetically constrained, thus requiring activation (directly or indirectly) from ATP hydrolysis (36). The Milo group developed a quantitative framework for the analysis of pathway thermodynamics. This simple thermodynamically derived metric, named the

max-min driving force (MDF) (32), can be used to compare the flux capacities permitted by pathway thermodynamics under physiological conditions. In this study, we applied the MDF metric using a pathway analysis tool, PathParser (31), to identify steps constrained by metabolite levels under physiological conditions. In the mevalonate pathway, the ACAT-catalyzed condensation of two acetyl-CoA into acetoacetyl-CoA is a thermodynamically constrained bottleneck step (Fig. 4). Based on calculation using eQuilibrator (37), this reaction has an estimated $\Delta G^{\circ\prime}$ of +26 kJ/mol (pH = 7.5; ionic strength of 0.2 M), indicating a highly unfavorable reaction. Our thermodynamic analysis indicates that this reaction operates near equilibrium under the optimized physiological conditions, and it easily becomes infeasible with the acetyl-CoA levels at the micromolar range found in eukaryotic cells (33) (Fig. 4; see also Tables S2 to S7 in the supplemental material). The mevalonate pathway is an important metabolic process found in all three kingdoms of life (38). How do cells then solve this conundrum under physiological conditions? A recent study has shed some light on this problem. In the methanogenic archaeon *Methanothermococcus thermolithotrophicus*, a large enzyme complex forms to connect ACAT with HMGS, the enzyme catalyzing the addition of a third acetyl-CoA to acetoacetyl-CoA to form (*S*)-3-hydroxy-3-methylglutaryl (HMG)-CoA in the mevalonate pathway (39). The enzyme complex forms a shared CoA binding site, allowing substrate channeling between the endergonic nondecarboxylative Claisen condensation and the exergonic HMG-CoA-forming reaction, substantially improving the thermodynamics of the mevalonate pathway. Indeed, when these two reactions are coupled, the overall reaction to convert three acetyl-CoA to HMG-CoA has an estimated $\Delta G^{\circ\prime}$ of +4.7 kJ/mol, calculated with eQuilibrator (37), which can be easily overcome by altering metabolite concentrations under physiological conditions. In the above-described study, genetic analysis also indicates the prevalence of this enzyme complex in archaea and in many bacteria, but not in eukaryotes (39). Standalone ACAT and HMGS are widespread in eukaryotes and some bacteria, which might explain the low terpene flux observed in these organisms. On the other hand, archaea have high demands for terpenoids as membrane lipids and require an efficient mechanism to overcome the highly unfavorable acetyl-CoA condensation reaction.

In eukaryotic thraustochytrids, cells seem to overcome the thermodynamic limitation of the nondecarboxylative Claisen condensation through a different mechanism. The mevalonate pathway has three ATP-dependent reactions downstream of mevalonate formation. In our study, respiration rates in *Thraustochytrium* sp. are significantly higher across the growth period in cells grown with sodium supplementation (Fig. 5C). Two ATP-dependent enzymes, MVK and MDD, in the mevalonate pathway are also significantly more abundant in cells grown with sodium supplementation. By enhancing ATP consumption in the lower part of the mevalonate pathway, it is thus possible to decrease the steady-state level of acetoacetyl-CoA and provide an overall favorable thermodynamic driving force for terpene synthesis under physiological conditions. In other studies, increasing ATP consumption has been successfully applied to drive thermodynamically unfavorable reactions (40, 41). It is also worth mentioning that although respiration rates are higher in cells grown with sodium, the intracellular ATP levels are maintained at similar levels under both growth conditions (Fig. 5B), showing an ATP homeostasis tightly regulated by balancing ATP production and consumption.

In order to accommodate the higher respiration needs, *Thraustochytrium* sp. cells seem to achieve this by shifting from carbohydrate metabolism to lipid oxidation to provide abundant reducing equivalents for the electron transport chain. Several key enzymes in the EMP pathway and pyruvate oxidation showed decreased levels in cells grown with sodium (Fig. 2). On the other hand, acyl-CoA dehydrogenase, the key enzyme in the β-oxidation pathway, had significantly higher abundance in cells grown with sodium. β-Oxidation bypasses the TCA cycle to generate reducing equivalents. Not only does it provide acetyl-CoA for terpene biosynthesis, but it also provides NADH and $FADH_2$ to directly participate in the electron transport chain for ATP production. For every three acetyl-CoA that enter the mevalonate pathway, cells need to

invest 3 ATP and 2 NADPH, which could explain why increased ATP production favors squalene synthesis in *Thraustochytrium* sp. In plants, extracellular ATP can also contribute to the activation of the MVA pathway by phosphorylating mevalonate kinase through an ATP receptor, P2K1 (42). However, it is not known whether the same mechanism exists in thraustochytrids.

It is well known that many terpenoids play important roles in stress response and osmotic adjustment (43, 44). *Thraustochytrium* sp. employs a sodium-dependent mechanism to induce higher respiration, resulting in increased terpenoid biosynthesis. However, it is currently unknown how sodium induces the energy metabolism shift. The metabolomic analysis suggests that it is the outcome of maintaining both central metabolism intermediates for amino acid biosynthesis and fulfilling energy generation requirement. A likely mechanism could implicate the Ca^{2+}-dependent energy activation mechanism. Calcium ions are important second messengers of cell metabolism and can stimulate ATP synthesis in mitochondria by activating diverse enzymes in the electron transport chain (45). The influx of Ca^{2+} into mitochondria through the Na^{+}/Ca^{2+} exchange channel in the mitochondrial membrane has been shown to activate ATP generation in mouse heart cells (46). In thraustochytrids, ion exchange channels are a major response mechanism for osmotic stress (24), which could alter intracellular Ca^{2+} levels and led to increased respiration in the mitochondria. However, the exact mechanism remains to be elucidated.

Enhancing terpene flux is critical for high terpene yield in metabolic engineering. Besides kinetic improvement, increasing overall thermodynamic driving force by increased acetyl-CoA input has led to enhanced terpene flux and high terpene yields (27, 47). We further show in this study that mevalonate-derived terpene biosynthesis is constrained by local thermodynamics, which could be relieved by enhanced ATP investment. Engineering energy metabolism for enhanced ATP flux could be an important solution for future terpene engineering efforts. Alternatively, implementing the substrate-channeling design found in archaea in a model eukaryotic system could be a viable solution to improve the thermodynamic landscape of the mevalonate pathway and terpene yield.

MATERIALS AND METHODS

Strain and medium. The *Thraustochytrium* sp. ATCC 26185 strain was purchased from the American Type Culture Collection (Manassas, VA). Cells were cultured at 28°C at 170 rpm in enriched medium (EM) consisting of 30 g/liter glucose, 2.5 g/liter yeast extract, 2 g/liter monosodium glutamate, 1 g/liter KCl, 5 g/liter $MgSO_4 \cdot 7H_2O$, 0.1 g/liter $NaHCO_3$, 0.3 g/liter $CaCl_2$, 0.3 g/liter KH_2PO_4, 3 mg/liter $FeCl_3$, 0.6 mg/liter $ZnSO_4 \cdot 7H_2O$, 8.6 mg/liter $MnSO_4 \cdot 7H_2O$, 0.26 mg/liter $CoCl_2 \cdot 6H_2O$, and 0.02 mg/liter $CuSO_4 \cdot 5H_2O$. The seed culture was prepared by inoculating a single colony in 100 ml of EM with 25 g/liter NaCl and was grown for 2 days at 28°C with 170 rpm. For all salt induction experiments, 0.3 optical density at 660 nm (OD_{660}) of the seed culture was inoculated into 100 ml of EM with or without supplementing 5 g/liter NaCl. Cell growth, squalene and total lipid contents, ATP levels, and oxygen consumption rates were measured by collecting cells at 24, 48, 60, and 72 h.

Squalene quantification. Cells (2 ml) were collected at each time point by centrifuging at 3,000 $\times$ *g* for 5 min. The cell pellet was resuspended by vortexing in 1 ml of chloroform-methanol (1:2 vol/vol) for 3 min. Cedrene (30 μg) was added to the mixture to serve as the internal standard, followed by the addition of 1 ml acetonitrile and 2 ml hexane. The solvent mixture was vortexed for 1 min and centrifuged at 3,000 $\times$ *g* for 2 min. The extracted squalene in the top hexane phase was then transferred into a new tube and adjusted to a final volume of 2 ml using hexane. Squalene contents were analyzed by gas chromatography-mass spectrometry (GC-MS) in a Trace 1300 ISQ quadrupole (QD) (Thermo Fisher Scientific) system connected with a Zebron GC column (ZB-5MSplus, 30 m $\times$ 0.25 mm $\times$ 0.25 μm). The GC oven temperature was held at 90°C for 1 min, followed by a temperature increase to 300°C at the rate of 25°C/min and a final temperature hold at 300°C for 5 min. Squalene concentration was determined by calculating against a standard curve with 15 ppm of cedrene as the internal standard. An additional quantification method was used to quantify squalene contents for cells grown under different growth conditions (no salt, 0.086 mol/liter NaCl, or 0.086 mol/liter KCl). In this case, squalene was separated using an HP-5ms ultrainert (UI) GC column (30m $\times$ 250 μm $\times$ 0.25 μm) connected to an Agilent 7890B gas chromatograph coupled with a flame ionization detector. The GC oven temperature was held at 90°C for 1 min, followed by a temperature increase to 300°C at the rate of 25°C/min and a final temperature hold at 300°C for 7 min.

Determination of total fatty acids. A 1-ml aliquot of cells was centrifuged at 10,000 $\times$ *g* for 2 min to collect the cell pellet. Chloroform-methanol (200 μl, 2:1 vol/vol) and 0.6 M HCl-methanol solution (300 μl) were added into the cell pellet, followed by the addition of 30 μg of cedrene as the internal

standard. The solvent mixture was vortexed for 1 min, then incubated in a 65°C water bath for 2 h. Following incubation, the mixture was cooled to room temperature. Hexane (1 ml) was then added to extract the total lipids by thoroughly vortexing for 1 min. Finally, phase separation was achieved by centrifuging at 5,000 rpm for 2 min. The top hexane phase was collected for GC-MS analysis in the Trace 1300 ISD QD system. The initial oven temperature was set to 50°C and maintained for 0.5 min, followed by a temperature increase to 180°C at the rate of 25°C/min and hold for 5 min. The temperature was raised again to 250°C at the rate of 5°C/min and held at 250°C for 10 min. The amounts of fatty acid components (C_{14}, C_{15}, C_{16}, C_{17}, C_{18}, and C_{22}) were calculated against the internal standard cedrene in the GC-MS analysis. Total fatty acids were calculated as the sum of all lipid components.

Shotgun proteomics. Comparative proteomics was conducted by collecting *Thraustochytrium* sp. cells grown with or without 5 g/liter of NaCl in the EM. About 10 OD of cells were collected at the time point of 60 h by centrifuging at 10,000 × *g* for 2 min. The proteomic sample preparation and mass spectrometry analysis in a Thermo LTQ Orbitrap XL mass spectrometer were conducted following the same protocol as that in our previous study (48). The raw data collected from tandem mass spectrometry (MS/MS) analysis were searched and analyzed using programs integrated into the PatternLab for Proteomics (49). Peptide information was obtained by searching against the database obtained from translating our transcriptomic data (data not published).

Metabolomics. Semiquantitative analysis of metabolites in the central metabolism were conducted at the West Coast Metabolomics Center located at the University of California, Davis. Six replicates of cells grown with or without NaCl (5 g/liter) were used for the analysis. During sample collection, 1 to 2 ml of *Thraustochytrium* sp. cells were quickly harvested by centrifuging at 10,000 × *g* for 30 s and subsequently frozen at −80°C for further metabolite analysis. During analysis, metabolites were separated in an Rtx-5Sil MS gas chromatography column (Restek Corporation, PA, USA) coupled to a time of flight mass spectrometer. Data processing was performed using ChromaTOF versus 2.32 (50). Comparison of cells grown with or without sodium was based on metabolite levels normalized to cell optical density.

***In silico* analysis of pathway thermodynamics.** The thermodynamic feasibility of squalene synthesis from both glycolysis and the β-oxidation of a short-chain fatty acid (hexanoyl-CoA) was evaluated using the pathway analysis tool PathParser (31). PathParser seeks to solve a max-min problem by maximizing the Gibbs energy change ($\Delta G'$) of the most thermodynamically unfavorable reaction in the pathway, which can be formulated as follows:

$$\max \min \left(-\Delta G_1^{'}, -\Delta G_2^{'}, \cdots, -\Delta G^{'m}\right)$$

$$\text{such that } \Delta G_i^{'} = \Delta G_i^{'\circ} + R \cdot T \cdot S \cdot \ln(c) \quad (i = 1, 2, \cdots, m)$$

$$\ln(c_{\min}) \leq \ln(c) \leq \ln(c_{\max})$$

where m is the number of reactions in a pathway, c is the concentration vector of metabolites involved, and S is the stoichiometric matrix of the pathway reactions. The standard Gibbs free energies ($\Delta G'^m$) were searched in eQuilibrator database (37) with intracellular pH and ionic strength set to 7.5 and 0.2 M, respectively. The lower and upper bounds of metabolite concentrations were constrained to range from 1 μM to 10 mM, following the approximate concentration scale of cellular metabolites (51). In addition, cofactor concentrations were fixed to approximate levels found in eukaryotic cells (33), which allowed a proper evaluation of target pathway thermodynamics with encoded constraints from the wider metabolic network (32). Specifically, the following cofactor concentrations were defined: ATP = 0.005 M, ADP = 0.0005 M, NAD = 0.001 M, NADH = 0.0001 M, NADPH = 0.0001 M, NADP = 0.0001 M, orthophosphate = 0.01 M, coenzyme A = 0.001 M, CO_2 = 0.00001 M, and diphosphate = 0.001 M.

Acetyl-CoA and ATP determination. Acetyl-CoA and ATP levels were monitored throughout the cell growth. About 1 OD of cells were collected by centrifuging at maximum speed for 15 s at 4°C. Cells were quenched by adding 1 ml of ice-cold methanol, followed by incubation for 1 h at −30°C. The extracted acetyl-CoA in the methanol solution was dried using a slow nitrogen stream and dissolved in deionized water. Acetyl-CoA levels were determined using the microorganism acetyl-CoA enzyme-limited immunosorbent assay (ELISA) kit (Mlbio, Shanghai, China) according to the manufacturer's instruction. The extracted ATP in the methanol solution was dried in a speed vacuum and dissolved in deionized water. ATP levels were determined using the ATP determination kit (Molecular Probes) according to the manufacturer's instruction.

Oxygen consumption rate. Cell respiration rates were determined by measuring oxygen consumption rates in a Clark-type oxygen electrode (Oxygraph system; Hansatech Instruments). Aliquots of cells (2 ml) grown with or without NaCl were collected at the time points of 24, 48, 60, and 72 h. No oxygen consumption was observed in the blank EM with or without the addition of NaCl. All cells were diluted to an OD of ~0.5 and monitored for 2 min at room temperature for oxygen consumption rates. The final oxygen consumption rates were normalized by cell optical density.

Data availability. The proteomics data have been deposited to the ProteomeXchange Consortium with the data set identifier PXD021931 (52).

SUPPLEMENTAL MATERIAL

Supplemental material is available online only.

FIG S1, TIF file, 2.1 MB.

FIG S2, TIF file, 0.6 MB.
TABLE S1, DOCX file, 0.01 MB.
TABLE S2, DOCX file, 0.01 MB.
TABLE S3, DOCX file, 0.01 MB.
TABLE S4, DOCX file, 0.02 MB.
TABLE S5, DOCX file, 0.02 MB.
TABLE S6, DOCX file, 0.01 MB.
TABLE S7, DOCX file, 0.02 MB.

ACKNOWLEDGMENTS

This work was supported by Miami University startup funds to X.W., National Science Foundation of China grants (91751115 and 31670044) to G.W., and a scholarship from the Chinese Scholarship Council to A.Z. This work was authored in part by the National Renewable Energy Laboratory, operated by the Alliance for Sustainable Energy, LLC, for the U.S. Department of Energy (DOE) under contract no. DE-AC36-08GO28308. This study was supported in part by funding provided by the Laboratory Directed Research and Development program (C.W., W.X.).

We thank Bo Wang for careful reading of the manuscript. We also thank Andor Kiss and Xiaoyun Deng of the Center for Bioinformatics and Functional Genomics at Miami University for instrument support.

The views expressed in the article do not necessarily represent the views of the DOE or the U.S. Government. The U.S. Government retains, and the publisher, by accepting the article for publication, acknowledges that the U.S. Government retains a nonexclusive, paid-up, irrevocable, worldwide license to publish or reproduce the published form of this work, or allow others to do so, for U.S. Government purposes.

REFERENCES

1. Wang X, Ort DR, Yuan JS. 2015. Photosynthetic terpene hydrocarbon production for fuels and chemicals. Plant Biotechnol J 13:137–146. https://doi.org/10.1111/pbi.12343.
2. Tholl D. 2006. Terpene synthases and the regulation, diversity and biological roles of terpene metabolism. Curr Opin Plant Biol 9:297–304. https://doi.org/10.1016/j.pbi.2006.03.014.
3. Tholl D. 2015. Biosynthesis and biological functions of terpenoids in plants. Adv Biochem Eng Biotechnol 148:63–106. https://doi.org/10.1007/10_2014_295.
4. Thimmappa R, Geisler K, Louveau T, O'Maille P, Osbourn A. 2014. Triterpene biosynthesis in plants. Annu Rev Plant Biol 65:225–257. https://doi.org/10.1146/annurev-arplant-050312-120229.
5. Rao CV, Newmark HL, Reddy BS. 1998. Chemopreventive effect of squalene on colon cancer. Carcinogenesis 19:287–290. https://doi.org/10.1093/carcin/19.2.287.
6. Ohkuma T, Otagiri K, Tanaka S, Ikekawa T. 1983. Intensification of host's immunity by squalene in sarcoma 180 bearing ICR mice. J Pharmacobiodyn 6:148–151. https://doi.org/10.1248/bpb1978.6.148.
7. Fox CB. 2009. Squalene emulsions for parenteral vaccine and drug delivery. Molecules 14:3286–3312. https://doi.org/10.3390/molecules14093286.
8. Deprez P, Volkman J, Davenport S. 1990. Squalene content and neutral lipid composition of livers from deep-sea sharks caught in Tasmanian waters. Mar Freshw Res 41:375–387. https://doi.org/10.1071/MF9900375.
9. Lombard J, Moreira D. 2011. Origins and early evolution of the mevalonate pathway of isoprenoid biosynthesis in the three domains of life. Mol Biol Evol 28:87–99. https://doi.org/10.1093/molbev/msq177.
10. Lange BM, Rujan T, Martin W, Croteau R. 2000. Isoprenoid biosynthesis: the evolution of two ancient and distinct pathways across genomes. Proc Natl Acad Sci U S A 97:13172–13177. https://doi.org/10.1073/pnas.240454797.
11. Vranova E, Coman D, Gruissem W. 2013. Network analysis of the MVA and MEP pathways for isoprenoid synthesis. Annu Rev Plant Biol 64:665–700. https://doi.org/10.1146/annurev-arplant-050312-120116.
12. Radisky ES, Poulter CD. 2000. Squalene synthase: steady-state, pre-steady-state, and isotope-trapping studies. Biochemistry 39:1748–1760. https://doi.org/10.1021/bi9915014.
13. Rodríguez-Concepción M, Boronat A. 2015. Breaking new ground in the regulation of the early steps of plant isoprenoid biosynthesis. Curr Opin Plant Biol 25:17–22. https://doi.org/10.1016/j.pbi.2015.04.001.
14. Özaydın B, Burd H, Lee TS, Keasling JD. 2013. Carotenoid-based phenotypic screen of the yeast deletion collection reveals new genes with roles in isoprenoid production. Metab Eng 15:174–183. https://doi.org/10.1016/j.ymben.2012.07.010.
15. Pollier J, Vancaester E, Kuzhiumparambil U, Vickers CE, Vandepoele K, Goossens A, Fabris M. 2019. A widespread alternative squalene epoxidase participates in eukaryote steroid biosynthesis. Nat Microbiol 4:226–233. https://doi.org/10.1038/s41564-018-0305-5.
16. Zhao C, Kim Y, Zeng Y, Li M, Wang X, Hu C, Gorman C, Dai SY, Ding S-Y, Yuan JS. 2018. Co-compartmentation of terpene biosynthesis and storage via synthetic droplet. ACS Synth Biol 7:774–781. https://doi.org/10.1021/acssynbio.7b00368.
17. Lewis TE, Nichols PD, McMeekin TA. 1999. The biotechnological potential of thraustochytrids. Mar Biotechnol (NY) 1:580–587. https://doi.org/10.1007/pl00011813.
18. Kaya K, Nakazawa A, Matsuura H, Honda D, Inouye I, Watanabe MM. 2011. Thraustochytrid *Aurantiochytrium* sp. 18W-13a accummulates high amounts of squalene. Biosci Biotechnol Biochem 75:2246–2248. https://doi.org/10.1271/bbb.110430.
19. Aasen IM, Ertesvåg H, Heggeset TMB, Liu B, Brautaset T, Vadstein O, Ellingsen TE. 2016. Thraustochytrids as production organisms for docosahexaenoic acid (DHA), squalene, and carotenoids. Appl Microbiol Biotechnol 100:4309–4321. https://doi.org/10.1007/s00253-016-7498-4.
20. Nakazawa A, Matsuura H, Kose R, Kato S, Honda D, Inouye I, Kaya K, Watanabe MM. 2012. Optimization of culture conditions of the thraustochytrid *Aurantiochytrium* sp. strain 18W-13a for squalene production. Bioresour Technol 109:287–291. https://doi.org/10.1016/j.biortech.2011.09.127.
21. Zhang A, Xie Y, He Y, Wang W, Sen B, Wang G. 2019. Bio-based squalene production by *Aurantiochytrium* sp. through optimization of culture conditions, and elucidation of the putative biosynthetic pathway genes. Bioresour Technol 287:121415. https://doi.org/10.1016/j.biortech.2019.121415.
22. Hoang MH, Ha NC, Thom LT, Tam LT, Anh HTL, Thu NTH, Hong DD. 2014. Extraction of squalene as value-added product from the residual biomass

of *Schizochytrium mangrovei* PQ6 during biodiesel producing process. J Biosci Bioeng 118:632–639. https://doi.org/10.1016/j.jbiosc.2014.05.015.
23. Patel A, Liefeldt S, Rova U, Christakopoulos P, Matsakas L. 2020. Co-production of DHA and squalene by thraustochytrid from forest biomass. Sci Rep 10:1–12. https://doi.org/10.1038/s41598-020-58728-7.
24. Shabala L, McMeekin T, Shabala S. 2009. Osmotic adjustment and requirement for sodium in marine protist thraustochytrid. Environ Microbiol 11:1835–1843. https://doi.org/10.1111/j.1462-2920.2009.01908.x.
25. Morabito C, Bournaud C, Maës C, Schuler M, Cigliano RA, Dellero Y, Maréchal E, Amato A, Rébeillé F. 2019. The lipid metabolism in thraustochytrids. Prog Lipid Res 76:101007. https://doi.org/10.1016/j.plipres.2019.101007.
26. Ghisla S, Thorpe C. 2004. Acyl-CoA dehydrogenases: a mechanistic overview. Eur J Biochem 271:494–508. https://doi.org/10.1046/j.1432-1033.2003.03946.x.
27. Rodriguez S, Denby CM, Van Vu T, Baidoo EE, Wang G, Keasling JD. 2016. ATP citrate lyase mediated cytosolic acetyl-CoA biosynthesis increases mevalonate production in *Saccharomyces cerevisiae*. Microb Cell Fact 15:48. https://doi.org/10.1186/s12934-016-0447-1.
28. Nelson DL, Lehninger AL, Cox MM. 2008. Lehninger principles of biochemistry. W. H. Freeman, New York, NY.
29. Jäpelt RB, Jakobsen J. 2013. Vitamin D in plants: a review of occurrence, analysis, and biosynthesis. Front Plant Sci 4:136. https://doi.org/10.3389/fpls.2013.00136.
30. Huang M, Bao J, Hallström BM, Petranovic D, Nielsen J. 2017. Efficient protein production by yeast requires global tuning of metabolism. Nat Commun 8:1131. https://doi.org/10.1038/s41467-017-00999-2.
31. Wu C, Jiang H, Kalra I, Wang X, Cano M, Maness P, Yu J, Xiong W. 2020. A generalized computational framework to streamline thermodynamics and kinetics analysis of metabolic pathways. Metab Eng 57:140–150. https://doi.org/10.1016/j.ymben.2019.08.006.
32. Noor E, Bar-Even A, Flamholz A, Reznik E, Liebermeister W, Milo R. 2014. Pathway thermodynamics highlights kinetic obstacles in central metabolism. PLoS Comput Biol 10:e1003483. https://doi.org/10.1371/journal.pcbi.1003483.
33. Park JO, Rubin SA, Xu Y-F, Amador-Noguez D, Fan J, Shlomi T, Rabinowitz JD. 2016. Metabolite concentrations, fluxes and free energies imply efficient enzyme usage. Nat Chem Biol 12:482–489. https://doi.org/10.1038/nchembio.2077.
34. Cleland WW. 1967. Enzyme kinetics. Annu Rev Biochem 36:77–112. https://doi.org/10.1146/annurev.bi.36.070167.000453.
35. Beard DA, Qian H. 2007. Relationship between thermodynamic driving force and one-way fluxes in reversible processes. PLoS One 2:e144. https://doi.org/10.1371/journal.pone.0000144.
36. Bar-Even A, Flamholz A, Noor E, Milo R. 2012. Thermodynamic constraints shape the structure of carbon fixation pathways. Biochim Biophys Acta 1817:1646–1659. https://doi.org/10.1016/j.bbabio.2012.05.002.
37. Flamholz A, Noor E, Bar-Even A, Milo R. 2012. eQuilibrator—the biochemical thermodynamics calculator. Nucleic Acids Res 40:D770–D775. https://doi.org/10.1093/nar/gkr874.
38. Miziorko HM. 2011. Enzymes of the mevalonate pathway of isoprenoid biosynthesis. Arch Biochem Biophys 505:131–143. https://doi.org/10.1016/j.abb.2010.09.028.
39. Vögeli B, Engilberge S, Girard E, Riobé F, Maury O, Erb TJ, Shima S, Wagner T. 2018. Archaeal acetoacetyl-CoA thiolase/HMG-CoA synthase complex channels the intermediate via a fused CoA-binding site. Proc Natl Acad Sci U S A 115:3380–3385. https://doi.org/10.1073/pnas.1718649115.
40. Lan EI, Liao JC. 2012. ATP drives direct photosynthetic production of 1-butanol in cyanobacteria. Proc Natl Acad Sci U S A 109:6018–6023. https://doi.org/10.1073/pnas.1200074109.
41. Patnaik R, Roof W, Young R, Liao J. 1992. Stimulation of glucose catabolism in *Escherichia coli* by a potential futile cycle. J Bacteriol 174:7527–7532. https://doi.org/10.1128/jb.174.23.7527-7532.1992.
42. Cho S-H, Tóth K, Kim D, Vo P, Lin C-H, Handakumbura P, Rivas-Ubach A, Evans S, Pasa-Tolic L, Stacey G. 2020. Activation of the plant mevalonate pathway by extracellular ATP. Research Square preprint archive. https://www.researchsquare.com/article/rs-61470/v1.
43. McLean-Bowen CA, Parks LW. 1982. Effect of altered sterol composition on the osmotic behavior of sphaeroplasts and mitochondria of *Saccharomyces cerevisiae*. Lipids 17:662–665. https://doi.org/10.1007/BF02535375.
44. Ivashkevich S, Apukhovskaia L, Vendt V. 1981. Effects of sterols having different chemical structure and squalene on osmotic resistance of erythrocytes. Biokhimiia (Moscow, Russia) 46:1420–1425.
45. Nakano M, Imamura H, Nagai T, Noji H. 2011. Ca^{2+} regulation of mitochondrial ATP synthesis visualized at the single cell level. ACS Chem Biol 6:709–715. https://doi.org/10.1021/cb100313n.
46. Aksentijević D, Karlstaedt A, Basalay MV, O'Brien BA, Sanchez-Tatay D, Eminaga S, Thakker A, Tennant DA, Fuller W, Eykyn TR, Taegtmeyer H, Shattock MJ. 2020. Intracellular sodium elevation reprograms cardiac metabolism. Nat Commun 11:1–14. https://doi.org/10.1038/s41467-020-18160-x.
47. Huang Y-Y, Jian X-X, Lv Y-B, Nian K-Q, Gao Q, Chen J, Wei L-J, Hua Q. 2018. Enhanced squalene biosynthesis in *Yarrowia lipolytica* based on metabolically engineered acetyl-CoA metabolism. J Biotechnol 281:106–114. https://doi.org/10.1016/j.jbiotec.2018.07.001.
48. Shinde S, Zhang X, Singapuri SP, Kalra I, Liu X, Morgan-Kiss RM, Wang X. 2020. Glycogen metabolism supports photosynthesis start through the oxidative pentose phosphate pathway in cyanobacteria. Plant Physiol 182:507–517. https://doi.org/10.1104/pp.19.01184.
49. Carvalho PC, Lima DB, Leprevost FV, Santos MD, Fischer JS, Aquino PF, Moresco JJ, Yates JR, 3rd, Barbosa VC. 2016. Integrated analysis of shotgun proteomic data with PatternLab for proteomics 4.0. Nat Protoc 11:102–117. https://doi.org/10.1038/nprot.2015.133.
50. Fiehn O, Wohlgemuth G, Scholz M, Kind T, Lee DY, Lu Y, Moon S, Nikolau B. 2008. Quality control for plant metabolomics: reporting MSI-compliant studies. Plant J 53:691–704. https://doi.org/10.1111/j.1365-313X.2007.03387.x.
51. Bar-Even A, Noor E, Flamholz A, Buescher JM, Milo R. 2011. Hydrophobicity and charge shape cellular metabolite concentrations. PLoS Comput Biol 7:e1002166. https://doi.org/10.1371/journal.pcbi.1002166.
52. Vizcaíno JA, Csordas A, del-Toro N, Dianes JA, Griss J, Lavidas I, Mayer G, Perez-Riverol Y, Reisinger F, Ternent T, Xu Q-W, Wang R, Hermjakob H. 2016. 2016 update of the PRIDE database and its related tools. Nucleic Acids Res 44:D447–D456. https://doi.org/10.1093/nar/gkv1145.